# Numerical investigation of diffuser solidity effect on turbulent airflow and performance of the turbocharger compressor

**Chehhat, A. , Si-Ameur, M. , Boumeddane, B. , Abo-Serie Abdelfatah, E. and Boulahrouz, S.**



**Original citation:**
Chehhat, A. , Si-Ameur, M. , Boumeddane, B. , Abo-Serie Abdelfatah, E. and Boulahrouz, S. (2016) Numerical investigation of diffuser solidity effect on turbulent airflow and performance of the turbocharger compressor. *Applied and Computational Mechanics*, volume 10 (2): 79-96

ISSN 1802-680X
ESSN 2336-1182

Publisher: University of West Bohemia, Pilsen

Applied and Computational Mechanics 10 (2016) 79–96

# Numerical investigation of diffuser solidity effect on turbulent airflow and performance of the turbocharger compressor

A. Chehhat[a,b,*], M. Si-Ameur[b], B. Boumeddane[c], E. Abo-Serie[d], S. Boulahrouz[a]

[a] *Mechanical Engineering Department, Faculty of Technology, Abbes Laghrour University, Khenchela, 40000, Algeria*
[b] *LESEI Laboratory, Faculty of Engineering, University of Batna, 05000, Algeria*
[c] *Mechanical Engineering Department, Faculty of Technology, Saad Dahleb University, Blida 0 9000, Algeria*
[d] *Coventry University, School of Mechanical, Aerospace and Automotive Engineering, Coventry, UK*

Received 13 July 2016; received in revised form 14 November 2016

**Abstract**

Low solidity diffuser in centrifugal compressors can achieve both high efficiency and wide operating ranges which is of great importance for turbocharger compressor. Low solidity is achieved by using a low chord to pitch ratio. In this work, a CFD simulation is carried out to examine the effect of solidity on airflow field of a turbocharger centrifugal compressor which consists of a simple-splitter impeller and a vaned diffuser. By changing the number of diffuser vanes while keeping the number of impeller blades constant, the solidity value of the diffuser is varied. The characteristics of the compressor are evaluated for 6, 8, 10 and 12 stator vanes which correspond to solidity of: 0.78, 1.04, 1.29 and 1.55, respectively. The spatial distribution of the pressure, velocity and turbulent kinetic energy show that the diffuser solidity has significant effect on flow field and compressor performance map. The compressor with a 6 vanes diffuser has higher efficiency and operates at a wider range of flow rate relative to that obtained with larger vans number. However a non-uniform flow at the compressor exit was observed with relatively high turbulent kinetic energy.


*Keywords:* CFD analysis, diffuser solidity, turbocharger, turbulent flow, vaned diffuser

## 1. Introduction

To meet the future engine emission legislations and efficiently use the fuel, automotive industries embarked on downsizing the engine while comprising a turbocharger to be able to deliver high power when necessary. However designing a turbocharger to meet the engine requirements is a challenging task. The turbocharger must not only meet the largest possible range of engine operating speed but also must have high posting pressure and efficiency, with less space and lower weight to be able have a competitive market. The three key components determining the behavior of the compressor stage are the rotor, the diffuser and the volute. The rotor serves as energy transmitter from the rotating shaft to the medium air being compressed. Rotor design has reached a level from which no much further improvements may be possible. Nevertheless, diffuser optimization offers significant prospects with less effort.

The diffuser has to convert much of the kinetic energy into pressure energy with minimum flow losses. Two types of diffuser are commonly used; vaneless and vaned diffusers. The vaneless diffuser is simple in design and cheaper and provides a wide range of operation however; it has lower efficiency due to its complex flow conditions and high turbulence. On the other hand,

*Corresponding author. Tel.: +213 664 613 872, e-mail: achehhat@gmail.com.

vaned diffuser guides the flow in the radial direction and the flow velocity can be further reduced relative to the vanelss diffuser and therefore higher efficiency and more compact geometry can be achieved. However the efficiency can drop significantly if the flow rate increases due to the large attack angle and consequently more losses. In this context, different numerical simulations and experimental measurements have been carried out to understand the physical phenomena related to the internal flow through the turbocharger compressor. Many researches have been undertaken to study the flow interaction between impeller and diffuser so far [15]. It is found from the literature that the study of the diffuser solidity effect on the performance of the turbocharger centrifugal compressor by varying the number of diffuser vanes has not been the focus of attention. Previous experimental study showed that the pinched diffuser and the modification of the volute tongue location affect the compressor efficiency and pressure lines at high speed [19]. Furthermore, two numerical studies have shown that the vaneless and open angle diffuser result in a wider stable operating range and higher efficiency [15]. The study of the air flow through the turbocharger compressor with dual volute design revealed that the dual volute design could separate the compressor into two regions that can be treated separately. The investigation confirmed that the dual volute design extends the stable operating range comparing with the single volute design [14]. The impeller-diffuser interaction in a centrifugal compressor has been studied by generating four different types of diffuser configurations, by varying the radial gap between the impeller and diffuser. It is shown that the dependence of the compressor stage efficiency is well correlated to such interaction [3].

Numerical studies can provide reliable results to predict the performance of two different volutes with the same impeller as good agreement with the experimental measurements in volutes, at least at moderate mass flow rates was proved [25]. It is well known that the turbulence and flow field studies, play major roles in the pressure variation through the compressor, in this subject, detailed flow measurements at inlet plane of a centrifugal compressor with a vaneless diffuser showed that four regions of high shear can be identified within the flow: within the blade wake, between the passage wake and jet, within the thickened hub boundary layer and between the blade wake secondary flow passage vortex [22]. This study confirmed also that each of these regions is associated with high turbulent kinetic energy, TKE. A comparison of turbulent models in CFD analysis of radial turbo machines when using FLUENT software, confirmed that the standard $k$-$\varepsilon$ and RNG $k$-$\varepsilon$ models are superior turbulence methods [1]. It can be observed from most of numerical studies that the number of diffuser vanes can affect the system performance as well as the flow field and turbulence in the turbocharger centrifugal compressor.

In order to analyze the effect of diffuser vanes number on the compressor performance, in this study four types of diffuser are investigated with the same impeller and volute, they only differ in their vanes number: 6, 8, 10 and 12. For this purpose, the commercial CFD software FLUENT is employed considering a steady state condition, for simulating the three-dimensional turbulent air flow through the full stage of a centrifugal compressor, used in a turbocharger of automobile diesel engine, It is found from the analysis that the diffuser solidity presents a considerable effect not only on the fluid flow and turbulence characteristics, but also on the performances and operating range of the turbocharger compressor.

## 2. The compressor geometry and operating conditions

The compressor impeller and diffuser CAD geometry has been constructed using GAMBIT software which is part of ANSYS [9]. The various components of the compressor are constructed individually and then assembled. A sketch of the main geometry of the compressor parts and

rotor angles are shown in Fig. 1. The compressor has a shrouded impeller that comprises 7 full blades and 7 splitter blades. The simulation was carried out for various diffuser solidity $q$ given by (1) which is defined as the ratio between the blade chord $c$ and the blade pitch $t$, where $Z_b$ is the blades number, see Fig. 1:

$$q = \frac{c}{t}, \quad t = 2\pi r_m / Z_b, \quad r_m = (r_i + r_o)/2. \tag{1}$$

The solidity was varied by changing the diffuser blade (vane) numbers. Four diffusers have been constructed with $6$, $8$, $10$ and $12$ airfoil vanes as shown in Fig. 2. The corresponding solidity is $0.78$, $1.04$, $1.29$ and $1.55$, respectively. The volute has a non-symmetrical cross section beginning from $0^\circ$ and ending at $360^\circ$ (when a tongue is located) with a conical discharge pipe that can be connected to engine intake manifold. The main dimensions are listed in Table 1. The flow simulation was examined at different impeller speeds $60$, $80$ and $100$ krpm. The compressor mass flow rate was identified by varying outlet pressure.

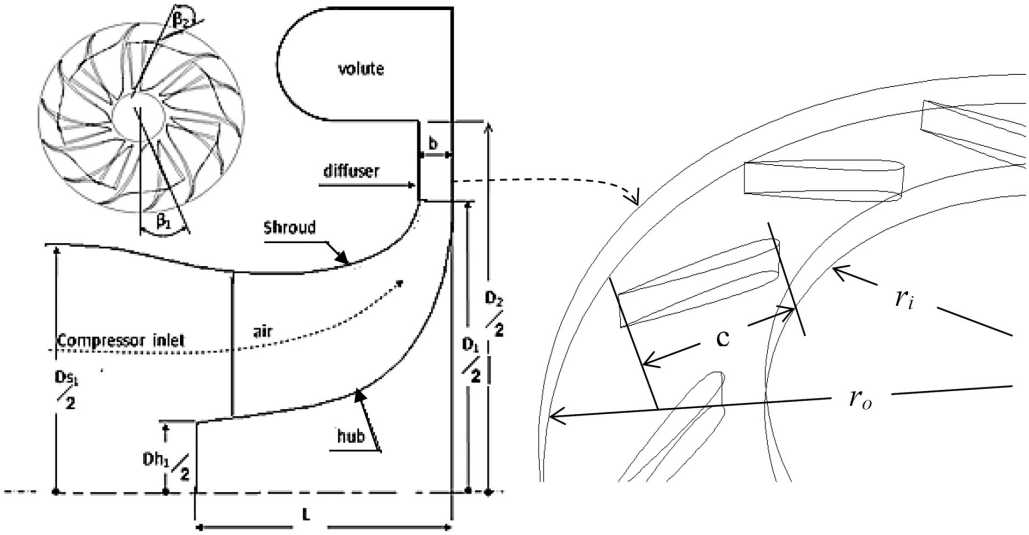


Fig. 1. Schematic of the centrifugal compressor stage geometry

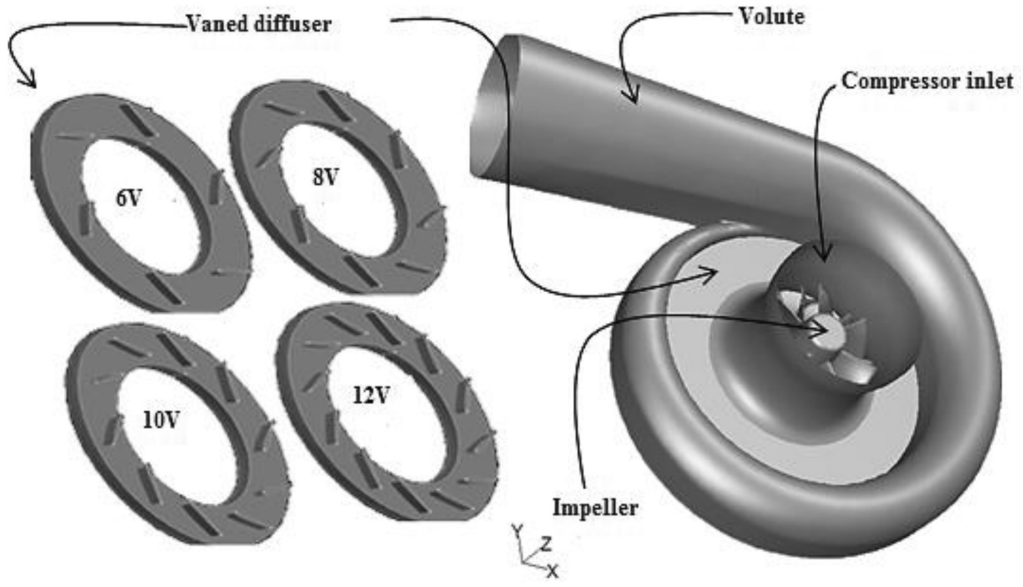


Fig. 2. Geometry model of vaned and vanless diffuser turbocharger compressor

Table 1. Geometrical dimensions of the compressor stage designed with GAMBIT software, see Fig. 1 for nomenclature

| Description | Symbol | Number/Dimension |
|---|---|---|
| Number of full impeller blades | $Z$ | 7 |
| Number of splitter impeller blades | $z_s$ | 7 |
| Impeller outlet diameter (m) | $D_1$ | 0.08 |
| Diffuser outlet diameter (m) | $D_2$ | 0.126 |
| Impeller outlet vane height (m) | $b$ | 0.004 5 |
| Inlet shroud diameter (m) | $D_{s1}$ | 0.068 |
| Inlet hub diameter (m) | $D_{h1}$ | 0.018 |
| Impeller axial length (m) | $L$ | 0.026 |
| Inlet mean line blade angle | $\beta_1$ | 50° |
| Outlet blade angle | $\beta_2$ | 30° |

## 3. Mathematical model

### *3.1. Reynolds Averaged Navier-Stokes equations*

The Reynolds Averaged Navier-Stokes (RANS) equations describe the statistic average component of turbulent flows; the instantaneous turbulent field is conventionally decomposed into an average component and a fluctuating component of zero average. For a steady state compressible flow, these equations are more specifically denoted as Favre averaged NS equations and presented in the following form:

#### *3.1.1. Continuity equation*

$$\frac{\partial}{\partial x_i}(\rho u_i) = 0. \tag{2}$$

#### *3.1.2. Momentum equation*

$$\frac{\partial}{\partial x_j}(\rho u_i u_j) = -\frac{\partial P}{\partial x_i} + \frac{\partial}{\partial x_j}\left[\mu\left(\frac{\partial u_i}{\partial x_j} + \frac{\partial u_j}{\partial x_i} - \frac{2}{3}\delta_{ij}\frac{\partial u_m}{\partial x_m}\right)\right] + \frac{\partial}{\partial x_j}\left[\mu_t\left(\frac{\partial u_i}{\partial x_j} + \frac{\partial u_j}{\partial x_i}\right) - \frac{2}{3}\left(\rho k + \mu_t\frac{\partial u_m}{\partial x_m}\right)\delta_{ij}\right], \tag{3}$$

where $\rho$ represents the density (kg m$^{-3}$), $u$ the velocity (m s$^{-1}$), $P$ the pressure (Pa), $k$ the turbulence kinetic energy (m$^2$ s$^{-2}$), $\mu$ the laminar viscosity (kg m$^{-1}$ s$^{-1}$), and $\mu_t$ the turbulent viscosity (kg m$^{-1}$ s$^{-1}$). The subscripts $i$, $j$ and $m$ represent the directions $x$, $y$, and $z$. The symbol $\delta_{ij}$ is the Kronecker delta, it is 1 when $i = j$, otherwise it is 0.

### *3.2. Energy equation*

$$\frac{\partial}{\partial x_i}[u_i(\rho E + P)] = \frac{\partial}{\partial x_j}\left(\kappa_{eff}\frac{\partial T}{\partial x_j} + u_i(\tau_{ij})_{eff}\right), \tag{4}$$

where $E$ is the total energy ($\mathrm{m^2\,s^{-2}}$), and $\kappa_{eff}$ is the effective thermal conductivity ($\mathrm{W\,m^{-1}\,K^{-1}}$). These quantities from the following equations:

$$E = h - \frac{P}{\rho} + \frac{u^2}{2}, \tag{5}$$

$$h = \int_{T_{ref}}^{T} c_P \,\mathrm{d}T, \quad T_{ref} = 288.15\,\mathrm{K}, \tag{6}$$

$$\kappa_{eff} = \kappa + \frac{c_p \mu_t}{\mathrm{Pr}_t}, \tag{7}$$

where $\kappa$ is the thermal conductivity of air ($\mathrm{W\,m^{-1}\,K^{-1}}$), and $c_p$ is the specific heat capacity of air ($\mathrm{J\,kg^{-1}\,K^{-1}}$). A constant value of $0.85$ is used for the turbulent Prandtl number $Pr_t$. The last term in (4) involves $(\tau_{ij})_{eff}$ which is the viscous stress tensor ($\mathrm{kg\,m^{-1}\,s^{-2}}$) and it is defined as

$$(\tau_{ij})_{eff} = (\mu + \mu_t)\left(\frac{\partial u_i}{\partial x_j} + \frac{\partial u_j}{\partial x_i} - \frac{2}{3}\delta_{ij}\frac{\partial u_m}{\partial x_m}\right). \tag{8}$$

### *3.3. Ideal gas equation*

The density variation in compressible flow was determined by the ideal gas equation:

$$\frac{P}{\rho} = RT, \tag{9}$$

$R$ is the gas constant ($\mathrm{J\,kg^{-1}\,K^{-1}}$) of air, and $T$ is the temperature (K).

### *3.4. $k$-$\varepsilon$ turbulence model*

The conservation equations for the TKE $k$ ($\mathrm{m^2\,s^{-2}}$) and its rate of dissipation $\varepsilon$ ($\mathrm{m^2\,s^{-3}}$) are calculated using $k$-$\varepsilon$ standard model. These two quantities are used to calculate the effect of the turbulence fluctuation components on the averaged conservation equations. The standard $k$-$\varepsilon$ model is simple and proves to be stable in predicting flow in turbocharger compressor [9]. Although $k$-$\varepsilon$ model has been used in most of the simulations, the results using RNG $k$-$\varepsilon$ and $k$-$\omega$ models have also been examined. The standard two-equation $k$-$\varepsilon$ turbulence equations are shown below:

$$\frac{\partial}{\partial x_i}(\rho k u_i) = \frac{\partial}{\partial x_j}\left[\left(\mu + \frac{\mu_t}{\sigma_k}\right)\frac{\partial k}{\partial x_j}\right] + G_k - \rho\varepsilon - Y_M, \tag{10}$$

$$\frac{\partial}{\partial x_i}(\rho \varepsilon u_i) = \frac{\partial}{\partial x_j}\left[\left(\mu + \frac{\mu_t}{\sigma_\varepsilon}\right)\frac{\partial \varepsilon}{\partial x_j}\right] + C_{1\varepsilon}\frac{\varepsilon}{k}G_k - C_{2\varepsilon}\rho\frac{\varepsilon^2}{k}, \tag{11}$$

where $\sigma_k$ and $\sigma_\varepsilon$ are the turbulent Prandtl numbers for $k$ and $\varepsilon$, and constant values of $1.0$ and $1.3$ are used, respectively. $G_k$ ($\mathrm{kg\,m^{-1}\,s^{-3}}$) represents the generation of turbulence kinetic energy due to the mean velocity gradients, and $Y_M$ ($\mathrm{kg\,m^{-1}\,s^{-3}}$) is the contribution of the fluctuating dilatation in compressible turbulence to the overall dissipation rate. They are calculated as

$$G_K = \left[\mu_t\left(\frac{\partial u_i}{\partial x_j} + \frac{\partial u_j}{\partial u_i}\right) - \frac{2}{3}\left(\rho k + \mu_t\frac{\partial u_m}{\partial x_m}\right)\delta_{ij}\right]\frac{\partial u_j}{\partial xi}, \tag{12}$$

$$Y_M = 2\rho\varepsilon\frac{k}{\gamma RT} \quad \text{and} \quad \gamma = \frac{c_P}{c_v}, \tag{13}$$

$Y_M$ is the contribution of the fluctuating dilatation to the dissipation rate (kg m$^{-1}$ s$^{-3}$), $\gamma$ is the specific heat ratio and $\mu_t$ is calculated as:

$$\mu_t = \rho\, C_\mu \frac{k^2}{\varepsilon}, \tag{14}$$

where $\sigma_k$ and $\sigma_\varepsilon$ are the turbulent Prandtl numbers for $k$ and $\varepsilon$, and constant values of $1.0$ and $1.3$ are used, respectively. The values of the model constants $C_{1\varepsilon}$, $C_{2\varepsilon}$ and $C_\mu$ are $1.44$, $1.92$ and $0.09$, respectively.

## 4. Numerical simulation

### *4.1. Model assumptions and settings*

The high complexity of the flow in the rotating impeller makes the CFD modeling difficult. Only steady state flow is investigated and accordingly three-dimensional Reynolds Averaged Navier-Stokes equation was discretized using the finite volume method, with the common algorithm in most commercial finite volume codes (pressure based implicit solver). The coupling velocity-pressure correction is treated with SIMPLE (Semi-Implicit Pressure Linked Equation) algorithm. The momentum and energy equations are solved using first order scheme, while the KE and dissipation rate equations are solved using the power low differencing scheme (PLDS). The fluid (air) was assumed to be compressible and treated as an ideal gas. To be able to have a stable solution and to avoid numerical divergence, the under relaxation factor for the pressure is taken $0.2$ while a value of $0.5$ is taken for the momentum, energy, and turbulence $k$-$\varepsilon$ model equations. The convergence is realized when the residual for all the governing equations reaches a value of $10^{-4}$. The maximum number of iterations was reached when the outlet mass flow rate remains constant.

### *4.2. Boundary conditions*

The meshed fluid domain has only one flow inlet (the compressor inlet) and one flow outlet (the volute exit). For the flow inlet, the pressure inlet boundary condition with atmospheric pressure (101 325 Pa) is taken as total pressure for the compressor entry, the total temperature is taken as the ambient (288 K), the default values of inlet TKE and its dissipation rate are taken $1.21$ m$^2$ s$^{-2}$ and $1.82$ m$^2$ s$^{-3}$, respectively. At the volute exit, the pressure outlet boundary condition is used with a prescribed static pressure (this value is determined by the engine operating conditions, it must be above the atmospheric pressure), the actual total temperature at the outlet is calculated or prescribed by the numerical simulation. At both the inlet and outlet, the default values of turbulent intensity and viscosity ratio are taken for the back-flow condition [15], which corresponds to the occurrence of reversed flow at the same grid cell faces of the outlet cross-section. Since for all the operating ranges no apparent reversed flow is observed when the simulation is converged.

### *4.3. Rotating region*

A Multiple Reference Frame (MRF) has been used to simulate the compressor flow. The flow domain has been divided into two regions, the rotating and fixed regions. The rotating region includes the impeller blades and the fluid that is surrounded by the impeller inlet surface, outlet surface, and a surface parallel to the shroud surface and located on the impeller blade surfaces parallel to the shroud surface. The rotating region is assigned to a rotating reference frame that

is rotating relative to the fixed reference with a speed equal to the impeller speed. The flow in each cell within the rotating region is solved using the moving reference frame equations. At the interfaces between the regions, a rotating reference frame transformation is performed to enable flow variables in one the rotating region to be used to calculate fluxes at the boundary of the fixed region.

### 4.4. Grid generation

Given the complexity of the compressor geometry, the full computational domain is meshed with tetrahedral grid cells, the clearance gap between the impeller and the diffuser is taken into consideration when meshing the impeller volume, near the impeller blade and diffuser vane walls. The mesh is refined as shown in Fig. 3.

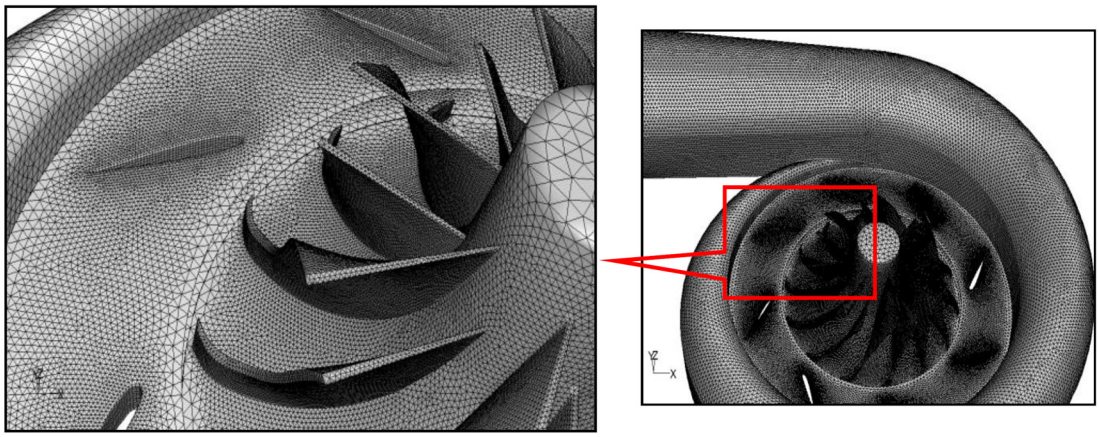

Fig. 3. Computational mesh of the vaned diffuser centrifugal compressor full sage

### 4.5. Independence grid-solution

In order to obtain a satisfactory solution, a grid independence study was carried out by comparing the radial distribution of the static pressure at half distance of the diffuser channel using five different grid sizes. The study was made for the lowest vane number (6 vanes) which contains the lowest grid cell number. As shown in Fig. 4, the trend of the static pressure with the radial distance is similar but with significant difference in magnitude for the case of 131 859 grid cells. To achieve reasonable accuracy with minimum computation time a grid of 252 192 grid cells has been used throughout all the simulations.

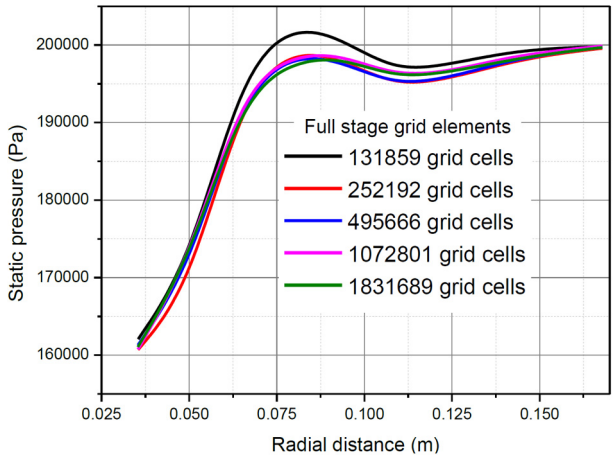


Fig. 4. Test of grid-solution independence

### 4.6. Turbulence model choice

In Fig. 5(a)–(b), the comparison of three RANS turbulence models $k$-$\varepsilon$, RNG $k$-$\varepsilon$ and $k$-$\omega$ is carried out to predict static and total pressure for the selected compressor, and it turned out that no major difference is seen between the three models with respect to their predictions of pressure. Except a slight deviation which is noticed after the diffuser where RNG $k$-$\varepsilon$ and $k$-$\omega$ are seem closer than $k$-$\varepsilon$ model. For this reason, the rest of results are performed using $k$-$\varepsilon$ model taking into account its easy convergence and fast computing.

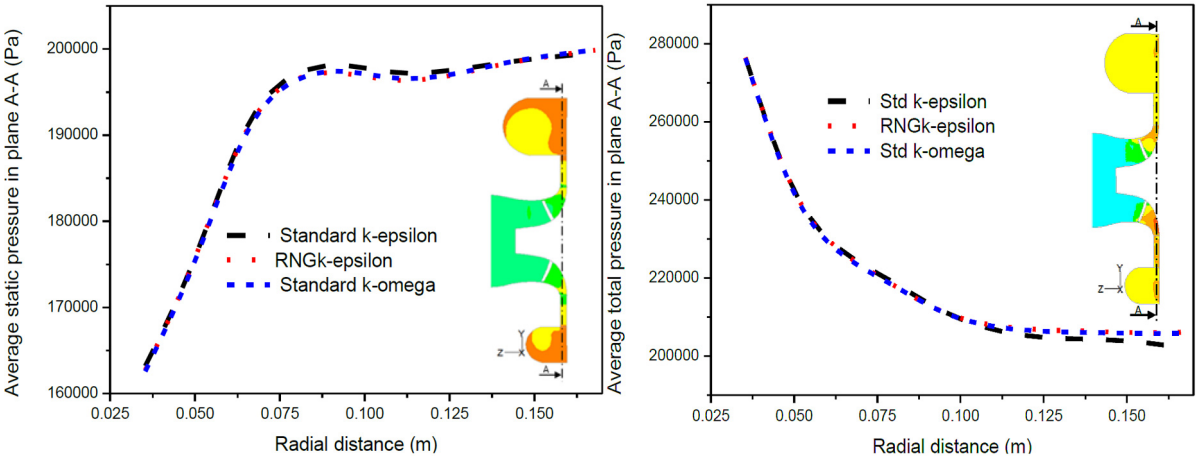


(a) static pressure (b) total pressure

Fig. 5. Static and total pressure predicted with three RANS models

### 4.7. CFD model validation

Before obtaining and discussing the results, it was necessary to validate the CFD model based on the experimental data available in the literature; the pressure ratio comparison study is shown in the Fig. 6a. The CFD calculations are compared with CFD results obtained by S. N. Danish [8] and experimentally tested turbocharger J90S-2 [13]. It can be seen that difference between our CFD and experimental results is less than 5 %, and this deviation may be explained by the fact that our CFD simulation does not match exactly include all dimensions as some dimensions of the tested compressor were missing and not available in open literature. That is why the calculated mass flow rate with the CFD model at a given outlet pressure is not the same as the real compressor. Fig. 6b shows same comparison but considering the compressor efficiency.

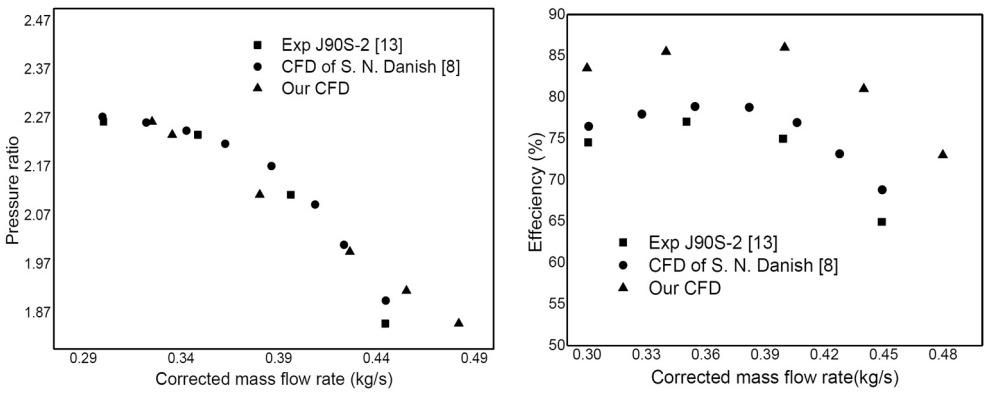


(a) pressure ratios (b) efficiencies

Fig. 6. Comparison of performances for vanless diffuser compressor

The compressor power is calculate by torque times the compressor angular speed. The torque was calculated by integrating the pressure and shear stress tangential component multiplied by the radius over all the impeller rotating surfaces. As seen in the figure, there is a significant difference between CFD results and experimental work. This deviation is more than that obtained from the comparison carried out for the static pressure case. Similar observations have been found by other researchers [17, 18]. The deviation can be attributed to many factors including the accurate geometrical representation for the small dimensions. Both comparisons are made for a vanless diffuser compressor which considered as a reference case at nominal rotational speed.

## 5. Results and discussions

### *5.1. Comparison of overall performance*

The average airflow rates for different compressor pressure ratios are calculated for each of the four diffusers and are presented in Fig. 7. The stage isentropic efficiency is also calculated and plotted in Fig. 7. The pressure ratio $\pi_c$ and isentropic efficiency $\eta_c$ are calculated on the basis of the total (stagnation) pressures $P_{\text{total}}$ and total (stagnation) temperatures $T_{\text{total}}$ at both inlet and outlet of the compressor, using the following relations:

$$\pi_c = \frac{P_{\text{total, outlet}}}{P_{\text{total, inlet}}}, \tag{15}$$

$$\eta_c = \frac{(\pi_c)^{0.285} - 1}{\tau_c - 1}, \tag{16}$$

$$\tau_c = \frac{T_{\text{total, outlet}}}{T_{\text{total, inlet}}}. \tag{17}$$

The air mass flow rate is corrected using the ambient conditions of temperature and pressure (288.15 K and 101 325 Pa) as follow:

$$Q_{\text{corrected}} = \frac{\sqrt{\tau_m}}{\pi_m} Q_{\text{real}}, \quad \tau_m = \frac{T_{\text{total,inlet}}}{288.15}, \quad \pi_m = \frac{P_{\text{total,inlet}}}{101\,325}, \tag{18}$$

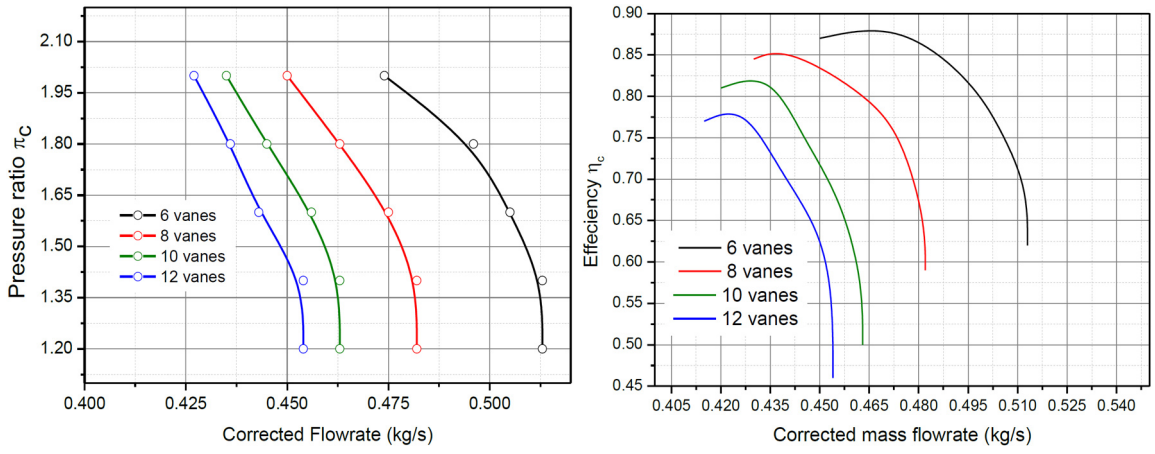


(a) pressure ratios (b) efficiencies

Fig. 7. Comparison of compressor performances for different diffuser vanes number

where, $Q_{\text{corrected}}$ and $Q_{\text{real}}$ are the corrected and real air mass flow rates, respectively, at the compressor inlet. $T_{\text{total, inlet}}$ and $P_{\text{total,inlet}}$ are the total (stagnation) temperature and pressure at the compressor inlet. It should be noted that the total temperature and pressure are the same as the reference values (288.15 K and 101 325 Pa); therefore the real and corrected air mass flow rates are identical for the simulations presented in this work. Fig. 8(a)–(b) shows the pressure ratio and efficiency versus the mass flow rate for different diffuser vane numbers. The figures show a significant change in the operating range and values of mass flow rate. Having fewer stator vanes results in shifting the operating rang of the compressor to higher mass flow rate and therefore can be more suitable for larger size or higher revolution engines. It is clearly seen that the significant increase in the peak efficiency value can be achieved by reducing the number of diffuser vanes. It can also be observed that the peak efficiency is achieved at higher air flow rate of about $0.46\,\text{kg}\,\text{s}^{-1}$ for the 6-vane diffuser relative to that from 8, 10 and 12 vanes diffuser which their peak efficiencies occur at about 0.44, 0.43, and $0.42\,\text{kg}\,\text{s}^{-1}$, respectively. As the number of vanes is reduced, the angle of diffusion of the airflow in each vane passage becomes larger. The larger diffusion angle results in more pressure recovery and higher static pressure at the exit of the diffuser vanes. Nevertheless, flow losses may increase due to poorer flow guidance relative to that with more vanes stator. In contrary, having the number of vanes increased results in reduction in the angle of diffusion and hence less static pressure conversion Nevertheless, less flow losses exists due to better guidance but is offset partially by skin friction losses due to the larger contact surfaces. Based on Fig. 8(a)–(b), it can be concluded that the pressure gained due to low number of vanes is exceeding the losses and therefore higher pressure and efficiency are obtained for the same flow rate. Generally there is always a need to arrive at a trade off with respect to the number of diffuser vanes considering the fluid guidance and friction effects in the vane passages [16].

Fig. 8a shows the peak efficiency and range variation versus the number of diffuser vanes. The figure shows a linear increase in the compressor peak efficiency as the number of vanes decreases to reach a maximum value of 87 % for a 6-vane diffuser which presents the lowest solidity. However, this increase is expected to flatten as the numbers of vanes are further decreased due to flow separation and its associated losses. The figure also shows that the optimum flow rate which is the flow rate corresponding to the peak efficiency increases with low number of diffuser vanes. The stable operating range which is a portion of the compressor curve corresponding to high efficiency points for the 6-vane diffuser is wider in comparison with the three other diffusers and it reaches almost 34 % more than the 12-vane diffuser as shown in Fig. 8b.

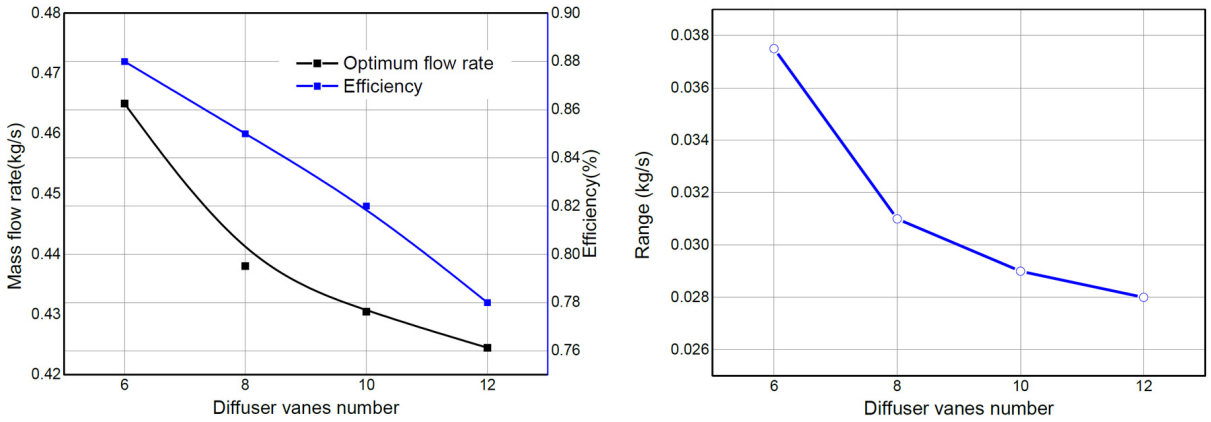


(a) efficiency and optimum mass flow rate (b) stable operating range

Fig. 8. Effect of diffuser vane number on compressor (a) efficiency and optimum mass flow rate and (b) stable operating range

### 5.2. Fluid flow characteristics

#### 5.2.1. Mean velocities distribution

Analyzing the obtained results, it is shown that the flow leaving the impeller has jets and wakes. When such a flow enters a large number of diffuser passages, the quality of flow entering the diffuser vanes varies widely and some of the vanes may experience flow separation leading to rotating stall and poor performance. To avoid such a possibility, it is safer to provide a smaller number of diffuser vanes than that on the impeller [22]. As explained in the previous section the number of vanes in the diffuser has a significant influence on the compressor efficiency and its range of operation. The variation in flow characteristics is attributed to the reduction in diffusion angle when the number of vanes increases and therefore affects the flow pattern in the diffuser area. Fig. 9 shows the stream lines plots mapped on colored velocity magnitude at optimum design mass flow rate condition for different stator vane number.

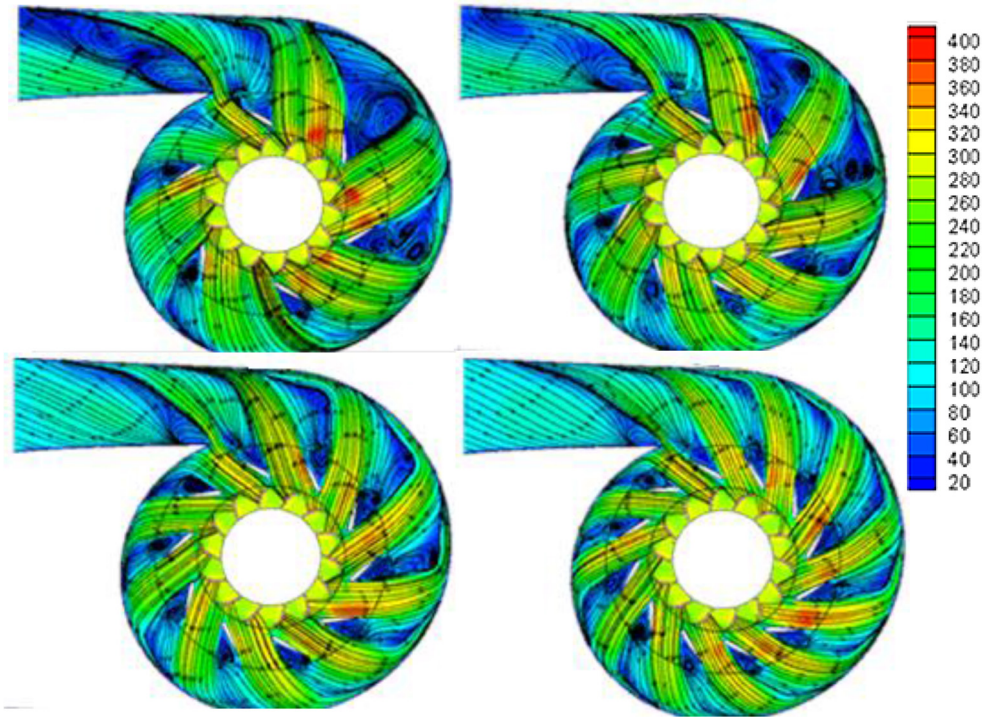


Fig. 9. Streamlines plots colored by velocity magnitude at design mass flow

The figure shows a small vortex located between each two consecutive vanes and therefore more number of smaller vortices can be found when using more number of vanes. On the other hand, the diffuser with lower number of vanes showed lower number of vortices with slightly larger size. Although larger vortices contains more energy but it is not necessarily all the energy are cascaded and converted to turbulence and dissipated before exiting the compressor outlet. Smaller vortices with smaller length and time scales have more dissipated energy fractions before exiting the compressor outlet. It is therefore possible to have the compressor flow domain with larger number of diffuser vanes to dissipate more energy. The reason of shifting the operating range to higher flow rate for lower vane diffuser can be attribute to the stalling phenomenon which is associated with the blade passing frequency. Having larger number of vanes on the diffuser results in an increase in the blade passing frequency. It can also be attributed to the narrower vane passages of the diffuser in which recirculation on the suction side of the diffuser

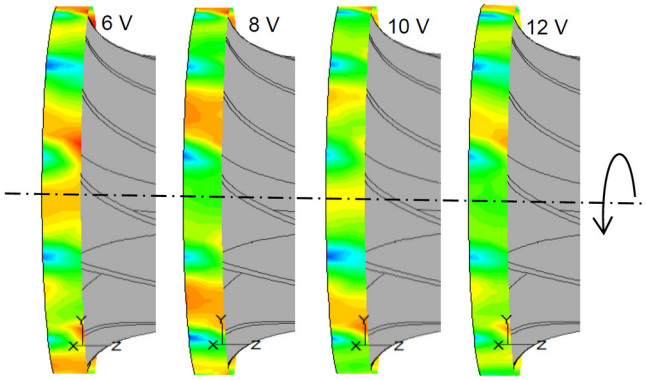


Fig. 10. Contours of meridional velocity at the impeller exit for four diffusers at design flow rate

vanes gets converted into a rotating stall [25]. In Fig. 10 contours of meridional velocity at the impeller exit for the four diffusers are shown. In this figure, the wake of the blade suction side near the shroud is clearly observed. The main blade wake is wider than that of splitter, which is similar to what has been observed in previous studies [21]. The figure shows that the velocity for lower vane stator has more meridional velocity gradient. The guidance by having more vanes leads to more uniformity of the flow.

Fig. 11 shows the velocity vectors plot on the meridional plane at design mass flow rate condition for four diffusers. The figure shows that the maximum velocity occurs at the impeller exit in agreement with previous studies [21]. Nevertheless, it can be observed that the magnitude of the velocity at the impeller exit is lower for low number of stator vanes compressor. Moreover, in all cases a recirculation zones is clearly seen in the rotor near the convex shroud. The convexity and high curvature of the shroud is responsible for the formation of steep adverse pressure gradient and the formation of such recirculation flow near the shroud. Similar results have been observer by other researchers [6]. Having smaller recirculation zone and weakened vortex for the 6-vane compressor leads to an improvement to the compressor efficiency as also seen in previous studies [26].

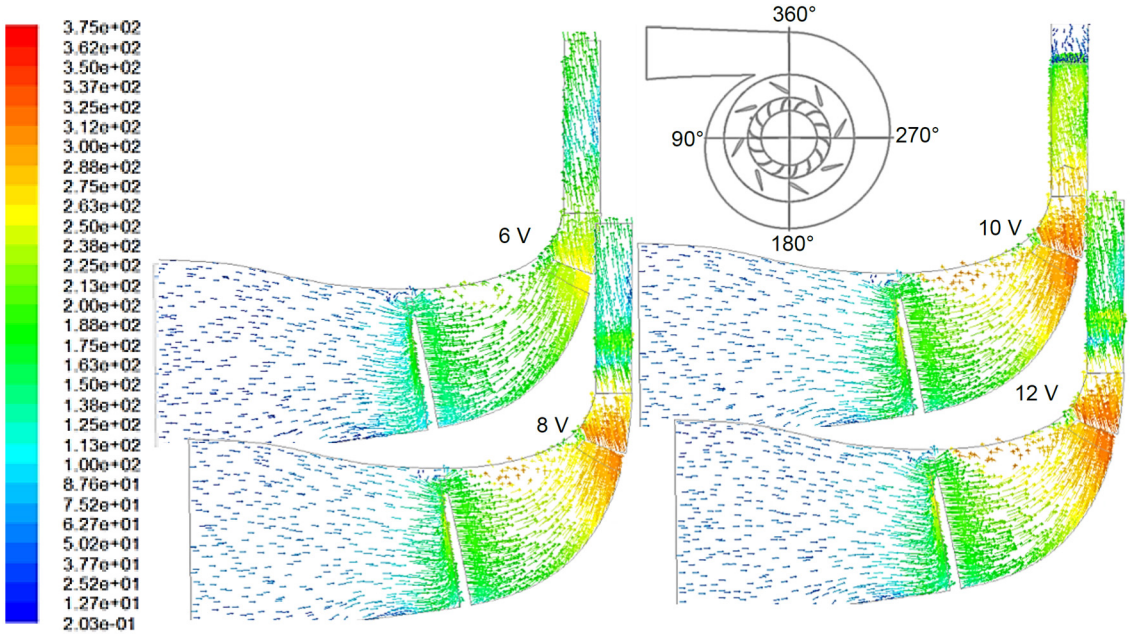


Fig. 11. Velocity vectors plot on the meridional plane (180°–360°) at design mass flow rate condition for four diffusers

### 5.2.2. *Pressure distribution*

Figs. 12 and 13 show the average of the circumferential static pressure at different radius taken over the iso-surface passing at half of the diffuser channel for the four diffusers. Three zones can be distinguished; impeller exit, diffuser and volute. At low flow rates, the static and total pressures were almost the same for the four diffusers. The static pressure increases rapidly as it exits the impeller and passes through the stator vanes and then slowly increases in the volute. At higher flow rates, the static pressure trend is significantly different from that for low flow rate due to the pressure loss particularly at impeller exit and diffuser inlet. The static pressure recovery in the diffuser vanes and volute occurs at shorter distance in the low number of vane diffuser while it takes longer distance inside the vanes and volute for larger number of vanes diffuser. The peak of the static pressure recovery always occurs after exiting the diffuser inside the volute. The high velocity of air at the diffuser exit for larger number of vanes may lead to longer vane wakes and therefore the flow has to travel longer distance to pass the vortex region and have the pressure recovered. After reaching the peak static pressure, the airflow mixing from all vanes became dominant and therefore a pressure loss occurs in this region. Further away from the mixing region the flow became more uniform and the volute diversion have more influence and therefore the static pressure increases while the total pressure is almost constant.

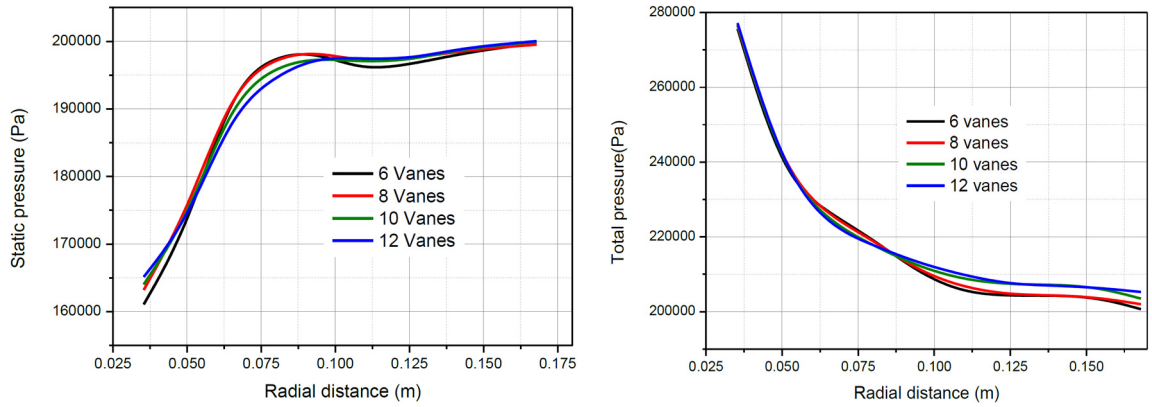


(a) static pressure (b) total pressure

Fig. 12. Circum-average-radial of (a) static and (b) total pressure at design flow rate condition for four diffusers

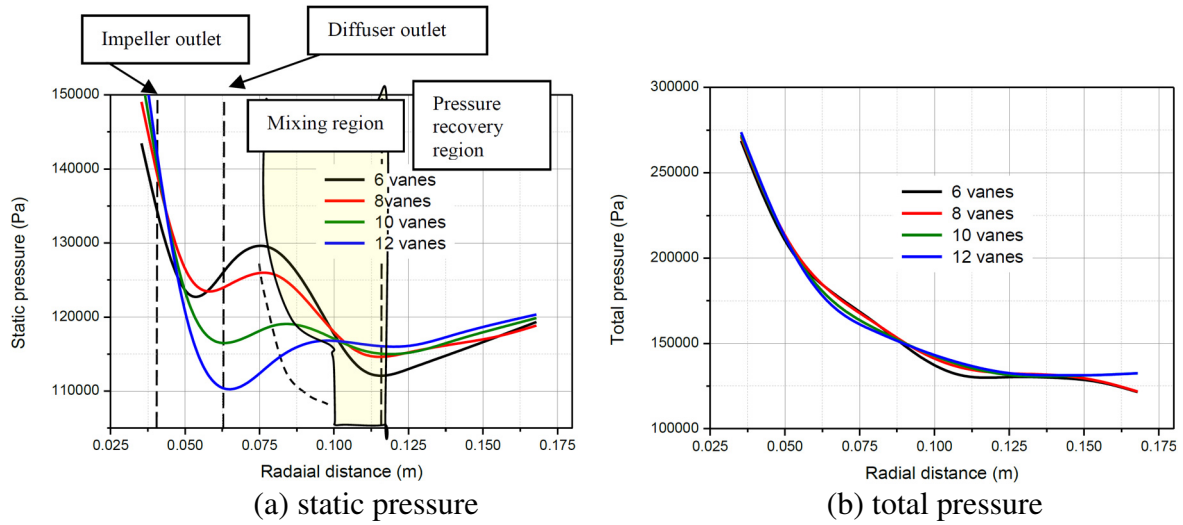


(a) static pressure (b) total pressure

Fig. 13. Circum-average-radial of (a) static and (b) total pressure at high flow rate condition for four diffusers

Fig. 14 shows the static pressure contour plots. It is clearly seen that for diffuser with lower number of vanes (6 vanes), static pressure at the diffuser exit is larger compared to diffuser with larger number of vanes (12 vanes) as a result of the larger diffusion angle. Similar to the results obtained in Fig. 14 the maximum pressure occurs downstream the diffuser vane exit. Since the lower number of vanes, the passage of the flow is wider and the formed vortex is also small as seen in Fig. 12, the rest of the through flow in the diffuser vane passage will not be affected much by the recirculation zone. Nevertheless, diffusion process will be affected due to lower flow guidance within passage.

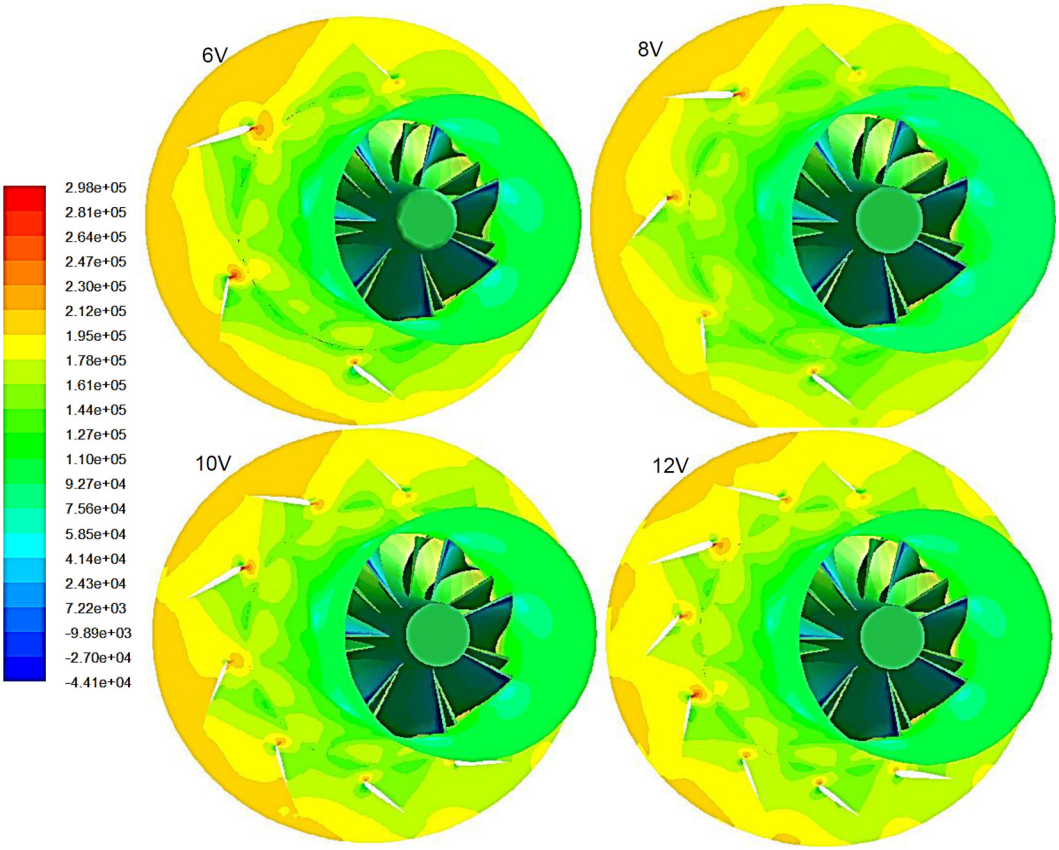


Fig. 14. Static pressure contours at design flow rate for four diffusers

### *5.3. Turbulent kinetic energy (TKE)*

Fig. 15 shows the Pathlines colored by TKE at design flow rate condition for the four diffusers, where it seems that high levels of TKE occurred not only in the rotor, but also close to the diffuser vanes. High level of TKE is also apparent at impeller blade inlet, as well as in blade wake and passage wakes, with slightly lower values. This behavior is in close agreement with [23]. Peak in TKE was still located to leading edge of diffuser vanes. Levels of kinetic energy were significantly dissipated in the compressor casing especially at volute outlet.

TKE levels in axial direction are not affected by the diffuser solidity, as shown in Fig. 16a for the lowest diffuser vane number (6 vanes) that is taken as a low solidity vaned diffuser (LSVD). In Fig. 16b the highest diffuser vane number (12 vanes) that is taken as a conventional vaned diffuser (CVD) showed no considerable change. While in radial direction, Figs. 17a and 17b at the design point and high flow rate conditions, respectively, the TKE magnitudes at

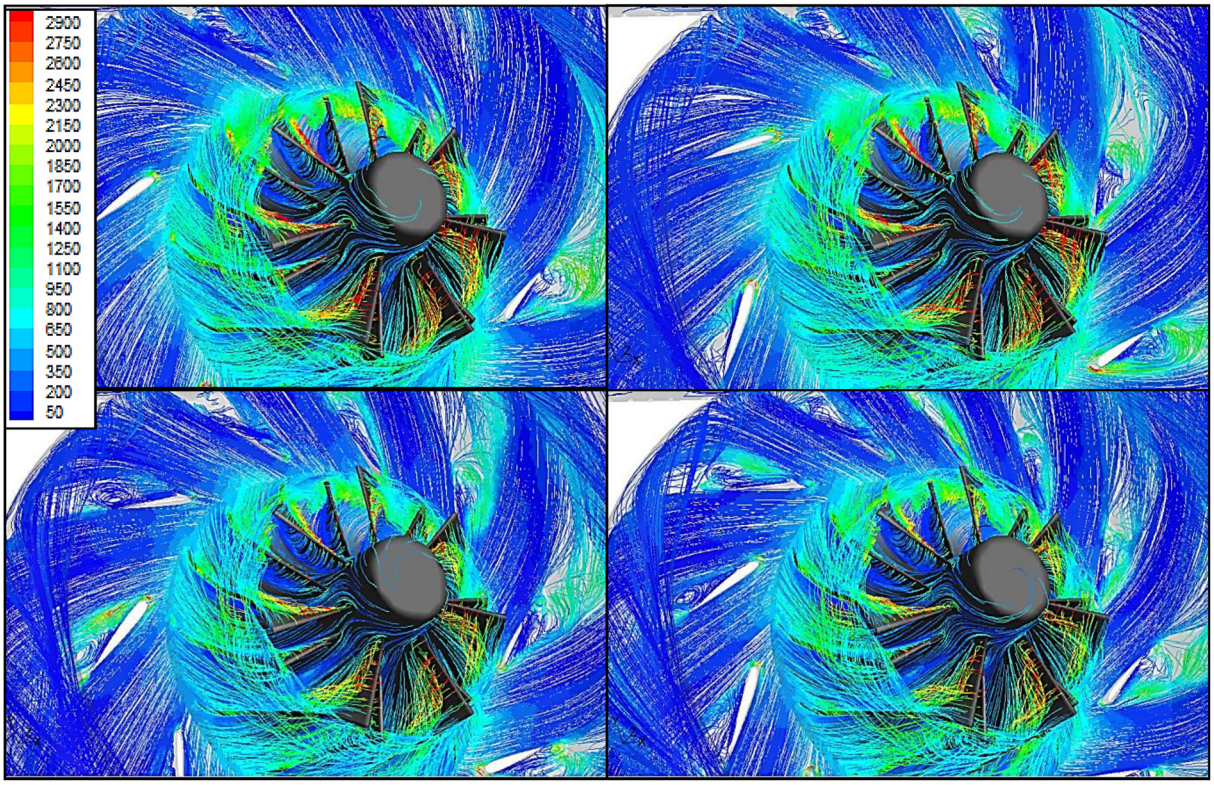


Fig. 15. Pathlines colored by TKE at design flow rate condition for four diffusers

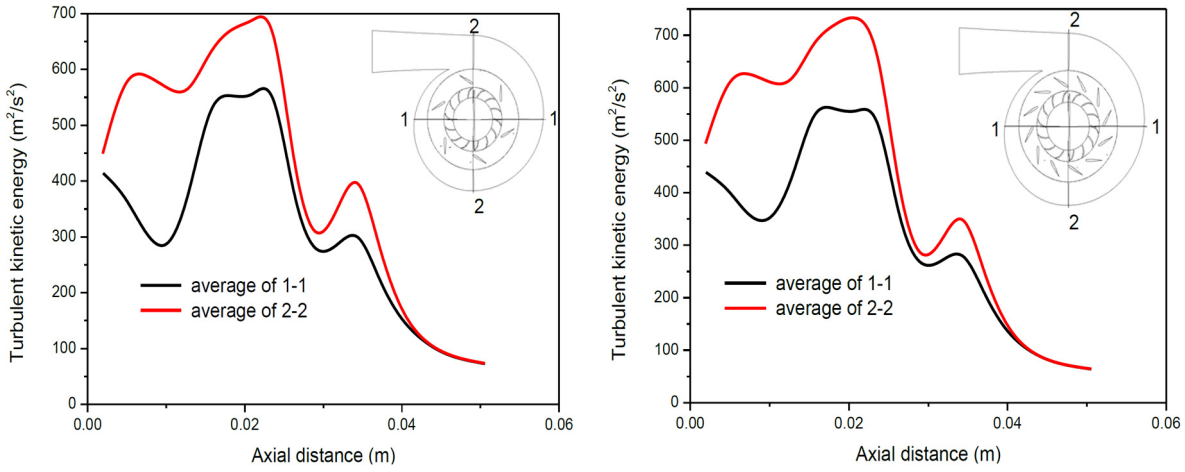


(a) CVD (b) LSVD

Fig. 16. Circumference-average-axial of TKE

larger radius for LSVD are higher even though, there is relatively lower average TKE exiting the diffuser (0.063 mm). On the other hand the diffusers with larger number of vanes have higher turbulent kinetic at the diffuser exit which dissipates and exits the compressor outlet with lower TKE. The energy dissipated insider the flow domain results in loss of fluid flow mechanical energy. The lower exit TKE for higher diffuser vane number is in agreement with other researchers [3].

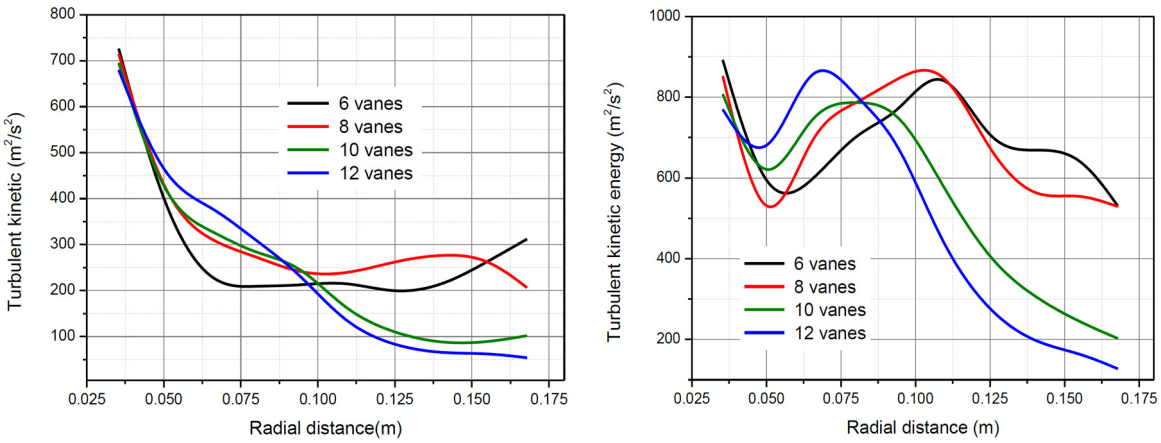


(a) design flow rate condition (b) high flow rate condition

Fig. 17. Circum-average-radial of TKE at high flow rate condition for four diffusers

## 6. Conclusions

In this work, a steady state computational fluid dynamics analysis of a shrouded centrifugal compressor used in turbocharger application is carried out considering four different diffusers of different solidity by varying their vanes number (6, 8, 10 and 12). Before the analysis is carried out the numerical results are compared with a previous CFD simulation and an experimental study to be able to have confidence in the model results. From this study, it can be concluded that:

1. The flow pattern of a turbocharger centrifugal compressor can be described with the moving reference frame (MRF) and the 3D RANS turbulence model, and valuable information can also be provided by analyzing the results, which can guide engineers in the design process.
2. The number of diffuser vanes has significant influence on the compressor performance. Having lower vanes (6 vanes) results in wider range of operation and shifts that range to higher flow rate. Moreover, the efficiency was improved.
3. A vortex located between each two consecutive diffuser vanes is generated and its size decreases as the number of vanes increases. It is found that the small vortices experiences more dissipation for its energy before exiting the compressor and thus, the flow leaves the compressor with relatively lower velocity fluctuations and lower TKE. On the other hand, the effect of larger vortex on the flow for lower number of vaned diffuser continued leading to non-uniform flow and higher TKE at the exit.
4. Four distinct regions have been identified for the circumferential average static pressure at different radius starting from the exit of the impeller at high flow rate. These regions are: the sharp pressure loss which occurs immediately at the impeller exit; the second is pressure recovery region; the third is a mixing region which is associated with pressure loss and the fourth is a pressure recovery that occurs in the volute.
5. There is a similarity between the circumferential average TKE and static pressure with similar four distinct regions except in the final stage where the static pressure increases while the TKE continue to decrease. Diffuser with large number of vanes results in lower TKE at the exit and volute.

6. The main turbulent features are detected by the numerical approach adopted in our study. The locations of the turbulent fluctuations are palpable and can have implications in engineering applications. However, the details near the walls need more refinement of the grid nodes which can have a great effect on the computational costs. Furthermore, another turbulence approaches should be used to explore this task in future works.

## Acknowledgements

The authors would wish to thank Dr. Georges Descombes from CNAM de Paris and Dr. Haitham Mezher from Ecole Central de Nantes (France) for their useful suggestions and worthy discussions about this work.

## References

[1] Aghaei tog, R., Toussi, A. M., Soltani, M., Design and CFD analysis of centrifugal compressor for a microgasturbine, Aircraft Engineering and Aerospace Technology 79(2) (2007) 137–143.

[2] Aghaei tog, R., Toussi, A. M., Tourani, A., Comparison of turbulence methods in CFD analysis of compressible flows in radial turbo machines, Aircraft Engineering and Aerospace Technology 80(6) (2008) 657–665.

[3] Anish, S., Sitaram, N., Computational investigation of impeller-diffuser interaction in a centrifugal compressor with different types of diffusers, Proceedings of the Institution of Mechanical Engineers, Part A: Journal of Power and Energy 223(2) (2009) 167–178.

[4] Bulot, N., Trébinjac, J., Ottavy, X., Kulisa, P., Halter, G., Paolitti, B., Krikorian, P., Experimental and numerical investigation of flow field in a high-pressure centrifugal compressor impeller near surge, Proceedings of the Institution of Mechanical Engineers, Part A: Journal of Power and Energy 223(6) (2009) 657–666.

[5] Chehhat, A., Si-Ameur, M., Boumeddane, B., CFD analysis of the volute geometry effect on the turbulent air flow through the turbocharger compressor, Energy Procedia 36 (2013) 746–755.

[6] Cumpsty, N. A., Compressor aerodynamics, Longman Scientific, University of Cambridge, 1999.

[7] Dai, Y., Engeda, A., Cave, M., Liberti, J.-L. Di, Numerical study and experimental validation of the performance of two different volutes with the same compressor impeller, Proceedings of the Institution of Mechanical Engineers, Part A: Journal of Power and Energy 223(2) (2009) 157–166.

[8] Danish, S. N., Qureshi, S. R., EL-Leathy, A., Khan, S., Umer, U., Chaochen, M., Numerical investigation & comparison of a tandem-bladed turbocharger centrifugal compressor stage with conventional design, Journal of Thermal Science 23(6) (2014) 523–534.

[9] Fluent 6.3 user's guide, 2006 (Fluent Inc., Lebanon, New Hampshire).

[10] Galindo, J., Serrano, J. R., Climent, H., Tiseira, A., Experiments and modelling of surge in small centrifugal compressor for automotive engines, Experimental Thermal and Fluid Science 32(3) (2008) 818–826.

[11] GAMBIT 2.2 user's guide, 2004 (Fluent Inc., Lebanon, New Hampshire).

[12] Guo, Q., Chen, H., Zhu, X.-C., Du, Z.-H., Zhao, Y., Numerical simulations of stall inside a centrifugal compressor, Proceedings of the Institution of Mechanical Engineers, Part A: Journal of Power and Energy 221(5) (2007) 683–693.

[13] J90S-2 turbocharger. Manufactured by Weifang Xinde Make Industry and Trade Co., Ltd, Shandong, China, http://wxmiatcl.en.china.cn.

[14] Jiao, K., Sun, H., Li, X., Wu, H., Krivitzky, E., Schram, T., Larosiliere, L. M., Numerical simulation of air flow through turbocharger compressors with dual volute design, Applied Energy 86 (2009) 2494–2506.

[15] Jiao, K., Sun, H., Li, X., Wu, H., Krivitzky, E., Schram, T., Larosiliere, L. M., Numerical investigation of the influence of variable diffuser angle on the performance of a centrifugal compressor, Proceedings of the Institution of Mechanical Engineers, Part D: Journal of Automobile Engineering 223(8) (2009) 1061–1070.

[16] Karanth, K. V., Sharma, N. Y., Numerical analysis on the effect of varying number of diffuser vanes on impeller — diffuser flow interaction in a centrifugal fan, World Journal of Modelling and Simulation 5 (2009) 63–71.

[17] Le Sausse, P., Fabrie, P., Arnou, D., Clunet, F., CFD comparison with centrifugal compressor measurements on a wide operating range, EPJ Web of Conferences 45 (2013) 01059-P.1-8.

[18] Leilei, W., Dazhong, L., Yixiong, L., Ce, Y., Non-axisymmetric flow characteristics in centrifugal compressor, Journal of Thermal Science 24(4) (2015) 313–322.

[19] Mohtar, H., Chesse, P., Chalet, D., Hetet, J. F., Yammine, A., Effect of diffuser and volute on turbocharger centrifugal compressor stability and performance: Experimental study, Oil & Gas Science and Technology — Rev. IFP Energies Nouvelles 66(5) (2011) 779–790.

[20] Nakagawa, K., Hayami, H., Keimi, Y., Comparison of two diffusers in a transonic centrifugal compressor, International Journal of Rotating Machinery 9 (2003) 279–284.

[21] Nili-Ahmadabadi, M., Hajilouy-Benisi, A., Durali, M., Ghadak, F., Investigation of a centrifugal compressor and study of the area ratio and tip clearance effects on performance, Journal of Thermal Science 17(4) (2008) 314–323.

[22] Pinarbasi, A., Turbulence measurement in the inlet plane of a centrifugal compressor vaneless diffuser, International Journal of Heat and Fluid Flow 30 (2009) 266–275.

[23] Tatar, O., Ozturk, A., Pinarbasi, A., Flow analysis in centrifugal compressor vaneless diffusers, Journal of Scientific & Industrial Research 67 (2008) 348–354.

[24] Xu, C., Muller, M., Development and design of a centrifugal compressor volute, International Journal of rotating machinery 3 (2005) 190–196.

[25] Yahia, S., Turbines, compressors and fans, 2nd edition, Tata Mc Graw Hill, 2005.

[26] Zhang, Y., Wang, C., Xinqian, Z., Zhuge, W., Wu, Y., Xu, J., Adaptive flow optimization of a turbocharger compressor to improve engine low speed performance, Journal of Mechanical Science and Technology 27(6) (2013) 1581–1587.